

An electrodynamic wave model for the action potential

Vitaly L. Galinsky*

Center for Scientific Computation in Imaging, University of California at San Diego, La Jolla, CA 92037-0854, USA

Lawrence R. Frank†

Center for Scientific Computation in Imaging, University of California at San Diego, La Jolla, CA 92037-0854, USA and

Center for Functional MRI, University of California at San Diego, La Jolla, CA 92037-0677, USA

(Dated: February 1, 2024)

An alternative to the standard Hodgkin-Huxley model for the axon action potential is presented. It is based upon our recently developed theory of electric field wave propagation in anisotropic and inhomogeneous brain tissues that has been shown to explain a broad range of observed coherent synchronous brain electrical processes. Here we demonstrate that this theory also explains the spiking behavior of single neurons, thus bridging the gap between the fundamental element of brain electrical activity (the neuron) and large scale coherent synchronous electrical activity. This new theory overcomes the limitations of the Hodgkin-Huxley model such as the inability to explain extracellular spiking, efficient brain synchronization, saltatory conduction along myelinated axons, and a variety of other observed coherent macroscopic brain electrical phenomena. We also show that the standard cable axon theory can be recovered by our approach using the very crude assumptions of the piece-wise homogeneity and isotropy, but the diffusion process that the cable equation describes is not capable of supporting the action potential propagation in a wide range of experimentally reported axon parameters.

I. INTRODUCTION

The Hodgkin and Huxley model for axonal electric signaling [1] is a cornerstone of modern neuroscience and serves as the basis for the development of a wide range of complex models of brain electrical communication. This model, and a host of variations (e.g., [2–5]), (hereafter collectively referred to as HH) is based on the postulate that axons possess multiple voltage gated channels that open and close in synchrony thereby producing a coherent persistent electrical wave or ‘spike’ traveling along the axon. In order to parameterize experimentally observed spikes in support of this view, HH developed a model described by a reaction-diffusion process. However, despite the general utility, and universal acceptance of this model, several incontrovertible facts suggest its incompatibility with observed brain electrical activity, such as its inability to account for extracellular spiking, efficient brain synchronization, and saltatory conduction along myelinated axons, to name just a few.

In retrospect, this should not be surprising, as the HH model was never derived from first physical principles, but was an *ad hoc* construction based on a very simple model motivated more by its flexibility than its adherence to any first physical principles of electrodynamics. After all, a general multiparametric reaction-diffusion equation constructed with multiple time constants, thresholds, and power laws can empirically fit a multitude of physical systems, including the hypothesized neuron with multiple voltage gated channels, even if it is not the correct physical model. That trouble was brewing should

have been evident from the fact that this asynchronous, seemingly incoherent spiking activity at scales of a single neuron appeared inconsistent with observed oscillatory and wave-like patterns that are coherent across a wide range of spatial and temporal scales [6]. Attempts to reconcile these seemingly incompatible views led to the development of networks of incoherently spiking neurons [7–9]. However, because the original HH model is too complicated to describe even relatively small networks, these networks models were modified to be based on a very simplified but now ubiquitous model of a leaky integrate-and-fire (LIF) neuron where a single threshold and time constant replaces all the multiple gates, currents, channels and thresholds [2–5, 10–12]. The unfortunate consequence is that, rather than reconciling the two views, they now became incompatible, as LIF equations do not have a mechanism for any type of non-linear resonance to generate the sustained coherent traveling waves characteristic of neuronal “spiking” [13].

The source of these difficulties can be traced back to the lack of an accurate physical model of electric field dynamics that includes wave propagation and interaction in the anisotropic and inhomogeneous neural tissues. In an effort to address this deficiency, we developed such a theory which predicted the existence of previously undiscovered weakly evanescent transverse cortical brain waves (WETCOW) generated at surfaces (or interfaces) in neural tissues as a direct consequence of their anisotropy and inhomogeneity. This theory was shown to describe a wide range of observed coherent macroscopic brain electrical activity, including extracellular spiking, hypersynchronous spiking and bursting, neuronal avalanches, and cortical wave loops [14–17]. However, although the relationship to wave propagation in single neurons was implicit in these papers, it was not demonstrated explicitly.

* vit@ucsd.edu

† lfrank@ucsd.edu

We do so in this current paper by applying the WET-COW theory to an analytical model of a single neuron with a lipid bilayer with an anisotropic membrane conductivity. The consequence is the generation of waves of multiple frequencies and wave numbers propagating in the lipid bilayer axonal membrane that create coherent nonlinear wave states consistent with the spatial-temporal characteristics of experimentally observed single neuron action potentials.

Further, having derived this directly from first principles that incorporate tissue properties, we are able to directly predict the well known observation that signals propagate faster along myelinated axons, a result not attainable with the HH model. From a broader perspective, the demonstration that these coherent persistent traveling non-linear waves are a consequence solely of the electromagnetic properties of the neuronal tissues suggests that it may be these waves that modify states of multiple cross-membrane channels, causing them to open and close, rather the other way around, which would be a fundamental shift in the understanding of brain signaling.

II. THEORY

The approach is similar to that developed in our general theory [13–20] and is as follows. We begin with the general form of electromagnetic activity (Maxwell’s equations), from which we derive the charge continuity equation in complex anisotropic and inhomogeneous tissues. This equation is then solved within a cylindrical geometry representation of an idealized neuron with an inhomogeneous and anisotropic membrane of finite thickness surrounded on its inner and outer surfaces by a homogeneous isotropically conducting fluids. The key here is the inclusion of a membrane conductivity tensor that provides a reasonable approximation to the electrical properties of a lipid bilayer. We then solve the simple linear problem which demonstrates the existence of surface waves even for this reduced solution. We then extend this to the more realistic non-linear problem and demonstrate the existence of surface waves whose spatiotemporal characteristics match those of observed data of neuronal spiking, though now derived from first principles and thus directly related to neuronal geometry and microstructure.

A. The charge continuity equation

In the most general form, a description of electromagnetic activity in axon can be formulated through Maxwell equations in a medium, that are appropriate both for extracellular and intracellular regions, [21, 22]

$$\nabla \cdot \mathbf{D} = \rho, \quad \nabla \times \mathbf{H} = \mathbf{J} + \frac{\partial \mathbf{D}}{\partial t} \quad \Rightarrow \quad \frac{\partial \rho}{\partial t} + \nabla \cdot \mathbf{J} = 0.$$

Using the electrostatic potential $\mathbf{E} = -\nabla\phi$, Ohm’s law $\mathbf{J} = \boldsymbol{\sigma} \cdot \mathbf{E}$ (where $\boldsymbol{\sigma} \equiv \{\sigma_{ij}\}$ is an anisotropic conductiv-

ity tensor), a linear electrostatic property for brain tissue $\mathbf{D} = \varepsilon \mathbf{E}$, assuming that the scalar permittivity ε is a “good” function (i.e. it does not go to zero or infinity everywhere) and making the change of variables $\partial x \rightarrow \varepsilon \partial x'$, the charge continuity equation for the spatial-temporal evolution of the potential ϕ can be written in terms of a permittivity scaled conductivity tensor $\boldsymbol{\Sigma} = \{\sigma_{ij}/\varepsilon\}$ as

$$\frac{\partial}{\partial t} (\nabla^2 \phi) = -\nabla \cdot \boldsymbol{\Sigma} \cdot \nabla \phi + \mathcal{F}, \quad (1)$$

where we have allowed for the influence of other sources by the inclusion of a source (or forcing) term \mathcal{F} , that may have both linear and nonlinear parts. This can be written in tensor notation as

$$\partial_t \partial_i^2 \phi + \partial_i (\Sigma_{ij} \partial_j \phi) = 0, \quad (2)$$

where repeating indices denotes summation.

B. The conductivity tensor of the lipid bilayer

As shown in our earlier work [14], the existence of electric field surface waves is predicated on the inhomogeneity and anisotropy of the neural tissues. Remarkably, though, this does not require an exceedingly accurate characterization of tissue microstructure. Rather, local average tissue parameterizations are sufficient to make accurate predictions of complex local and long-range non-linear wave propagation properties. This is an important point, as there is a huge body of literature focused on suggesting the need for very accurate complex tissue models to accurately predict observed coherent macroscopic electromagnetic brain activity. As demonstrated in our previous publications, this is not the case [13–20].

The same holds true for the single axon case considered here, where a reasonable model for the membrane conductivity tensor $\boldsymbol{\Sigma}^m$ can be constructed using a set of pretty general assumptions and results in the generation of surface waves in the lipid membrane. First, it is assumed that both the along-axon (i.e., axial z) and across-axon (i.e., radial r) electric fields will generate currents not only along the electric field direction (i.e., along z and r , respectively) but will also generate currents that are perpendicular to the field (i.e., along r and z , respectively). That is, for radial (along r) fields $\Sigma_{rz} \neq 0$ and for axial (along z) fields $\Sigma_{rz} \neq 0$. Based only on these symmetry considerations, the membrane conductivity tensor $\boldsymbol{\Sigma}^m$ is assumed to have the following non-diagonal, asymmetric form

$$\boldsymbol{\Sigma}^m = \begin{pmatrix} \Sigma_{rr}(\phi) & \Sigma_{rz}(\phi) \\ \Sigma_{zr}(\phi) & \Sigma_{zz}(\phi) \end{pmatrix}, \quad (3)$$

where we indicate the fact that Ohm’s law inside the membrane is non-linear by adding a dependence of the conductivity tensor components on scalar potential ϕ . The currents generated parallel to the field are not expected to be equal (i.e. $\Sigma_{rr} \neq \Sigma_{zz}$) nor would be equal the currents generated perpendicular to the field ($\Sigma_{rz} \neq \Sigma_{zr}$).

C. Axon model

Both equations (1) and (2) are appropriate for anisotropic and inhomogeneous media in general geometry. However, for the purposes of this paper it is sufficient to consider an idealized model for an axon represented by a cylindrical shell of diameter d created by a membrane of thickness δ (that for myelinated axons includes the thickness of the myelin layers as well) that separates two homogeneous isotropically conducting fluids inside and outside of the shell with scaled conductivities $\Sigma^i = \sigma_i/\varepsilon_i$ and $\Sigma^e = \sigma_e/\varepsilon_e$. The conductivity inside the thin membrane is highly anisotropic and is specified in tensor form of the axially symmetric conductivity tensor Σ^m given by (3).

Experimental measurements have shown that extracellular and intracellular conductivities are similar to that of sea water (~ 4 S/m), or more exactly in the range from 0.28 S/m to 2.9 S/m for extracellular σ_e and intracellular σ_i [21, 22], and permittivities ε_e and ε_i are around 7×10^{-10} F/m. Thus both Σ^i and Σ^e are very large, on the order of 10^{10} Hz.

The conductivity of the membrane is significantly smaller. The values vary and can be assumed to be in the range from as low as 10^{-13} S/m or as high as 10^{-5} [21], with typical values around 10^{-9} S/m [22]. With comparable or slightly smaller values for the membrane dielectric permittivity $\varepsilon_m \sim 10^{-11}$ F/m it gives for the membrane scaled conductivity $|\Sigma|$ range estimate from 10^{-2} to 10^2 Hz, hence the ratio of the conductivities of the membrane and the extracellular/intracellular media is as small as 10^{-8} to 10^{-12} .

Because of this significant difference in scaled conductivities between the membrane and the surrounding fluids, for the analysis of electrodynamic processes near the membrane in the frequency range characteristic of axonal signaling it can be reasonably assumed that both extracellular and intracellular fluids act as very good (even perfect) conductors that keep the potential drop across the membrane at the resting potential value of $-V_0$ ($V_0 \sim 65$ mV). This allows using all variables normalized to the resting potential and scaled conductivity tensor of the internal fluids. Specifically, all the variables in equations (1) and (2) are normalized as $r \rightarrow r/d$, $\Sigma_{ij} \rightarrow \Sigma_{ij}/\Sigma^i$, $t \rightarrow t\Sigma^i$, and $\phi \rightarrow \phi/V_0$. We will also introduce normalized frequencies ($\omega \rightarrow \omega/\Sigma^i$) and radial ($\kappa \rightarrow \kappa d$) and axial ($k \rightarrow kd$) wave numbers that will be used later. For the normalized membrane thickness ($\bar{\delta} \rightarrow \delta/d$) it will be assumed that $\bar{\delta} < 1$. Often the difference between d and δ is significant so that $\bar{\delta} \ll 1$.

A simplified schematic picture of this anisotropic electric field – electric current geometry is shown in Fig. 1, although it is shown not to scale as $\bar{\delta} \ll 1$ and all the anisotropic currents should be shown in the very thin boundary layer and not far outside of the $1 \leq r \leq 1 + \bar{\delta}$ ring. Nevertheless, the schematics can be useful to emphasize the highly anisotropic structure of the voltage-current relationship when the membrane interface is

present.

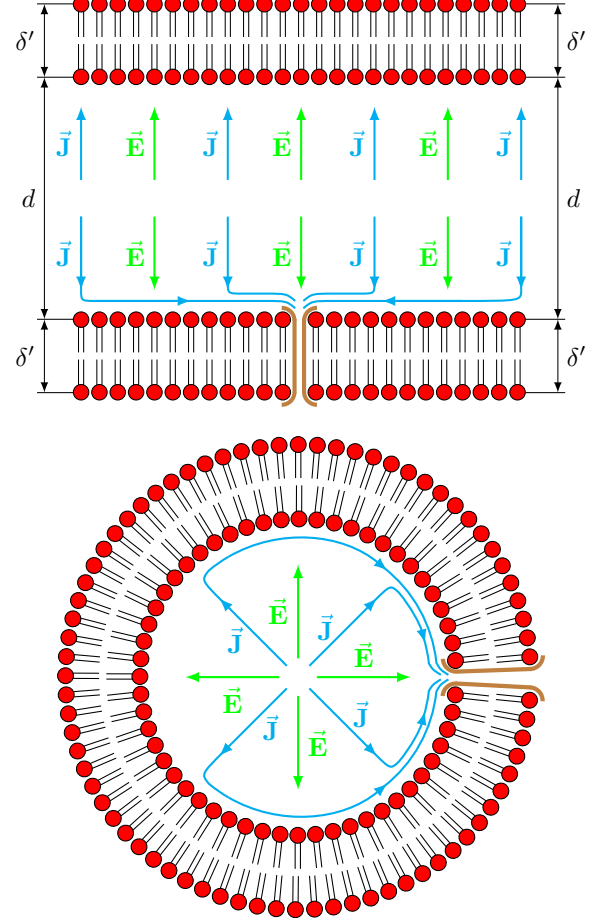


FIG. 1. Schematic picture of an axial (top) and a radial (bottom) sections of the axon. A radial component of an electric field \vec{E} inside the axon produces only a radial component of a current \vec{J} with typical isotropic conductivity. But a presence of cross-membrane channels results in appearance of non isotropic dependence of current as a response to a supplied electric field, giving rise to axial (top) and azimuthal (bottom) components of the current.

D. Solutions to the field equations

The solution to the charge continuity equation (2) within this anisotropic and inhomogeneous axon geometry is all that is required to explain the generation of surface waves that propagate through the extracellular-intracellular membrane interface. We emphasize that this is a derivation from first physical principles, in contradistinction to the standard model constructed from multiple empirical equations with multiple empirically fitted constants [1]. To simplify the math in a similar fashion as our previously published work [14] and provide a more intuitively clear result, we will assume the axon to be described by an axially symmetric cylindrical geometry

[21], although, generally speaking, for $\bar{\delta} \ll 1$ this is not absolutely necessary.

Defining

$$\mathbf{u} \equiv \begin{pmatrix} \frac{1}{r} \frac{\partial}{\partial r} r \\ \frac{\partial}{\partial z} \end{pmatrix}, \Sigma \equiv \begin{pmatrix} \Sigma_{rr} & \Sigma_{rz} \\ \Sigma_{zr} & \Sigma_{zz} \end{pmatrix}, \mathbf{v} \equiv \begin{pmatrix} \frac{\partial \phi}{\partial r} \\ \frac{\partial \phi}{\partial z} \end{pmatrix} \quad (4)$$

equation (1) can be written for a single axon in cylindrical (r, z) coordinate system as

$$\frac{\partial}{\partial t} (\mathbf{u}^t \cdot \mathbf{v}) = -\mathbf{u}^t \cdot \Sigma \cdot \mathbf{v} \quad (5)$$

Because of the huge difference in scaled conductances inside and outside of the bilayer membrane, the assumption of perfectly conducting boundary condition on both sides of the membrane bilayer is accurate and explicit solutions for the extracellular and the intracellular space are not required. It is only necessary to solve equation (5) inside the ring $1 \leq r \leq 1 + \bar{\delta}$. We will seek the solution in the form

$$\phi(r, z, t) = \phi^0(r) + \phi'(r, z, t), \quad (6)$$

$$\phi^0(r) = \frac{\ln r}{\ln(1 + \bar{\delta})} \approx \frac{1}{\bar{\delta}} \ln r, \quad (7)$$

where $\phi^0(r)$ is a stationary, time independent (or equilibrium) solution of the equation (5) inside the ring $1 \leq r \leq 1 + \bar{\delta}$, such that $\phi^0(r) \leq 1$ anywhere inside the ring whereas outside the ring $\phi^0(r) = 0$ for $r \leq 1$ and $\phi^0(r) = 1$ for $r \geq 1 + \bar{\delta}$.

The solution to the field equations can be approached at two levels of accuracy, a simplified but intuitive linear version, and a more accurate but complex non-linear version, by formally expanding the nonlinear dependence of the conductivity tensor in dimensionless form into Taylor series as

$$\Sigma(\phi) = \Sigma^0 + \frac{V}{V_0} \Sigma' \phi + \dots, \quad (8)$$

$$\text{where } \Sigma^0 \equiv \Sigma(\phi)|_{\phi=0} \quad \text{and} \quad \Sigma' \equiv \left. \frac{\partial \Sigma(\phi)}{\partial \phi} \right|_{\phi=0} \quad (9)$$

where (8) has been constructed with an adjustable normalization V to facilitate the inclusion of external conditions such as those prevalent in a wide range of experiments. For example, it can be set to the equilibrium value of a voltage drop across the membrane for voltage clamping experiments.

Without a loss of generality we can assume that the zeroth order terms are axisymmetric, with average dimensionless cross membrane conductivity $0 < \Sigma_{rr}^0 \equiv \Sigma^0 \ll 1$, average conductivity along the membrane (that possibly is significantly smaller) $\Sigma_{zz}^0 = \epsilon \Sigma_{rr}^0$ ($\epsilon < 1$), and zero off-diagonal terms $\Sigma_{rz}^0 = \Sigma_{zr}^0 = 0$, i.e.,

$$\Sigma^0 = \Sigma^0 \begin{pmatrix} 1 & 0 \\ 0 & \epsilon \end{pmatrix}. \quad (10)$$

With this positive definite matrix form used for Σ^0 the only solution that can be obtained from the equation (5) will correspond to the loss of the electrostatic field energy in the membrane. In order to be able to compensate for this loss and to keep the potential difference across the membrane at a fixed “resting potential” level some additional mechanisms are required. In axons this happens by adding energy through ATP-mediated diffusion. For the purpose of this paper, we are not interested in the details of this process and we will just assume that it provides required amount of energy to keep the cross membrane voltage drop at a constant level.

Because of the different concentrations of the different ions in extracellular and intracellular fluids (in particular, sodium and potassium ions), it has been known for a long time that nonlinear membrane properties show a positive feedback effect for the radial current-voltage relationship [21]. In terms of the nonlinear passive response produced by the conductivity tensor it means that some of the Σ' components are negative. At the same time the structure of Σ' should guarantee that there is neither total (volume integrated) additional electrostatic energy loss nor total electrostatic energy generation produced due to this nonlinear self coupling, therefore both eigenvalues of Σ' should be zeros (the eigenvalues of the conductivity matrix are real). As membrane conductivity is normalized by Σ^i , we would require that $|\Sigma_{\{\dots\}}| \leq 1$, and will assume that both $|\Sigma_{\{\dots\}}^0|$ and $|\Sigma'_{\{\dots\}}|$ are less than 1. This limits the structure of Σ' to the following form

$$\Sigma' = \Sigma' \begin{pmatrix} s_{\perp} xy & -s_{\parallel} x^2 \\ s_{\parallel} y^2 & -s_{\perp} xy \end{pmatrix}, \quad (11)$$

where $\Sigma' = \max |\Sigma'_{ij}|$, $\max(x, y) = 1$, $\min(x, y) \geq 0$, and both s_{\perp} and s_{\parallel} can either be -1 or 1. As we will see below, the choice of s_{\parallel} between -1 and 1 is not particularly important, as it simply selects different directions of wave propagation, but the different choice for a sign of s_{\perp} selects different scales where wave excitation and/or damping occurs, that experimentally has been noted as a different behavior of spiking for Type I and Type II neurons.

Based on experimental results that we cited above [21, 22], the normalized linear membrane conductivity is expected to be significantly less than 1 ($|\Sigma_{\{\dots\}}^0| \sim 10^{-8} - 10^{-12} \ll 1$). Therefore, the assumption for the first order normalized membrane conductivity that $|\Sigma'_{\{\dots\}}| < 1$ does not require it to be smaller than the linear normalized membrane conductivity, on the contrary it may be expected that $1 > |\Sigma'_{\{\dots\}}| \gg |\Sigma_{\{\dots\}}^0|$.

The solution for the second term $\phi'(r, z, t)$ in equation (6) can be expanded using radial and axial eigenmodes of the linearized system, with perfectly conducting boundary conditions at $r = 1$ and $r = 1 + \bar{\delta}$ that require that $E_z = 0$ or $\phi_r(1) = \phi_r(1 + \bar{\delta}) = 0$.

$$\phi_r(r) \sim R_0(\kappa r + \eta), \quad \phi_w(z, t) \sim e^{-i(\omega_k t + kz)}, \quad (12)$$

where R_0 denotes Bessel functions either of the first (J_0) or the second (Y_0) kind, and κ and η can be determined from the boundary conditions, $R_0(\kappa + \eta) = R_0(\kappa(1 + \bar{\delta}) + \eta) = 0$. Note that the parameters κ in $\phi_r(r)$ plays a similar role as the axial wave number k in $\phi_w(z, t)$ as larger values produce shorter wavelength spatial oscillations, but in the radial direction (although we are not interested in different radial modes and simply assume an existence of the longest mode with $\kappa\bar{\delta} \sim 1$). The derivative of radial eigenmode can then be written

$$\frac{d\phi_r}{dr} \sim -\kappa R_1(\kappa r + \eta), \quad (13)$$

where again R_1 denotes Bessel functions either of the first (J_1) or the second (Y_1) kind, and $R_1(\kappa + \eta) \approx \pm R_1(\kappa(1 + \bar{\delta}) + \eta)$.

Proceeding in a spirit similar to our earlier analysis [14], we first solve the simpler linear wave analysis problem by considering only the linear terms in equation (8) which are independent of z and t , then expand the scope of the analysis to include the non-linear terms that depend on z and t .

E. Linear wave analysis and surface wave generation

The linear in $\phi'(r, z, t)$ terms in equation (5) that are independent of z and t include from equation (8) $\Sigma_{\{\dots\}}^0$, that are constant inside the membrane layer, and $\Sigma'_{\{\dots\}}\phi^0(r)$, that only depend on radius r . Substituting the eigenmode solutions (12) into (5), multiplying by $\phi_r(r)r$, and integrating the radial part across the membrane bilayer, we obtain the complex dispersion relation

$$i\Omega_k \equiv \gamma_k + i\omega_k = \Lambda_{\perp} + i\Lambda_{\parallel}k \quad (14)$$

and the real Λ_{\perp} and the imaginary $i\Lambda_{\parallel}k$ parts of the dispersion correspond to the diagonal and the off diagonal conductivity tensor components,

$$\gamma_k \equiv \Lambda_{\perp} = (\gamma_d - \gamma_e), \quad (15)$$

$$\gamma_d = \frac{\Sigma^0}{\varkappa^2} (\kappa^2 + \epsilon k^2), \quad (16)$$

$$\begin{aligned} \gamma_e &= \hat{V}\Sigma' \frac{s_{\perp}xy}{\varkappa^2} \frac{(\kappa^2 C_{\perp}^r - k^2 C_{\perp}^z)}{\bar{\delta}C} \\ &\approx \hat{V}\Sigma' \frac{s_{\perp}xy}{2\varkappa^2} (\kappa^2 - k^2), \end{aligned} \quad (17)$$

$$\Lambda_{\parallel} = \hat{V}\Sigma' \frac{C_{\parallel}}{2\bar{\delta}C} \frac{s_{\parallel}(x^2 + y^2)}{\varkappa^2} \approx \hat{V}\Sigma' \frac{s_{\parallel}(x^2 + y^2)}{2\bar{\delta}\varkappa^2}, \quad (18)$$

in which $\hat{V} \equiv V/V_0$ is the fractional voltage (i.e., the fraction of the resting potential occupied by the external voltage) and

$$\varkappa^2 \equiv \kappa^2 + k^2 \quad (19)$$

The normalization parameters C_{\perp} , C_{\parallel} , and C are provided in Appendix 1 by (53). The parameter \varkappa^2 can be viewed as the length (squared) of a vector $\boldsymbol{\varkappa} = \boldsymbol{\kappa} + \mathbf{k}$ in an abstract vector space that controls the spatial scale of oscillations in the radial and longitudinal (axial) coordinates of the axon. The component Λ_{\perp} describes the damping (γ_d) or excitation (γ_e) of the waves while Λ_{\parallel} is related to the wave oscillations ω_k . Expressions (16) and (18) can be approximated as

$$\Lambda_{\perp} \approx \Sigma^0 \left[\left(\hat{\kappa}^2 + \epsilon \hat{k}^2 \right) + \hat{\sigma}_{\perp} \left(\hat{k}^2 - \hat{\kappa}^2 \right) \right] \quad (20)$$

$$\Lambda_{\parallel} \approx \Sigma^0 \frac{\hat{\sigma}_{\parallel}}{\bar{\delta}\varkappa^2}, \quad (21)$$

where $\hat{\kappa} \equiv \kappa/\varkappa$ and $\hat{k} \equiv k/\varkappa$ are the fractional wave numbers and

$$\hat{\sigma}_{\perp} \equiv \frac{1}{2} \hat{V} \hat{\Sigma} s_{\perp} xy \quad (22)$$

$$\hat{\sigma}_{\parallel} \equiv \frac{1}{2} \hat{V} \hat{\Sigma} s_{\parallel} (x^2 + y^2) \quad (23)$$

where $\hat{\Sigma} \equiv \Sigma'/\Sigma_0$ is the fractional conductivity (i.e., the ratio of the conductivity perturbation magnitude to the mean membrane conductivity). The parameters $\hat{\sigma}_{\perp}$ and $\hat{\sigma}_{\parallel}$ are the weightings for the (fractional) radial and longitudinal wave vector contributions to the radial and parallel components, respectively, of the dispersion relation. Each is scaled by both the fractional voltage and the fractional conductivity. The radial and longitudinal are scaled, respectively, by $s_{\perp} = \pm 1$ and $s_{\parallel} = \pm 1$ that have been introduced to demonstrate the profoundly different wave characteristics possible within the available parameter ranges of (14).

1. The existence of waves

This solution to the simplified linear problem is sufficient to show a key result - the existence of propagating surface waves along the axon. To see this, note that for large k ($k \gg \kappa$) that $\varkappa \approx k$ so from (21), $\Lambda_{\parallel} \sim 1/k^2$ so that the oscillatory component of the dispersion relation (14) is approximately $\omega_k = \Lambda_{\parallel}k \sim 1/k$ and thus exhibits the same inverse proportionality of frequency and wave number shown in our previous work [14, 15] (using Cartesian geometry) to generate surface (or interface) electric field waves. The relative magnitude of the conductivity tensor components in (8) are such that $1 > |\Sigma'_{\{\dots\}}| \gg |\Sigma^0_{\{\dots\}}|$ so that $\hat{\Sigma} \gg 1$ and thus the fractional conductivities (22) and (23) provide sufficiently large parameter ranges within the membrane to support wave excitation.

2. Wave characteristics

The parameters $s_{\parallel} = \pm 1$ and $s_{\perp} = \pm 1$ were introduced to delineate the profoundly different parameter regions

of the dispersion relation (14). This can now be shown directly using (21) and (20).

First consider the parallel component s_{\parallel} . Note that phase velocity of the waves is defined as $\omega_k/k = \Lambda_{\parallel}$ and thus determined by (21). Changing the sign of the s_{\parallel} changes the sign of σ_{\parallel} in (23) and thus changes the sign of the phase velocity (21). That is, it changes the direction of the wave propagation.

Now consider the perpendicular component s_{\perp} . Its influence on the solution provides an important new understanding of the role of the Nodes of Ranvier. Changing sign of s_{\perp} will change the sign of the wave excitation rate γ_e (17), i.e., it will result in two different wave excitation patterns. If s_{\perp} is positive, $\gamma_e > 0$ when $k < \kappa$, i.e., waves with longer wave length will be excited, which corresponds to Type I myelinated axons, where longer wave lengths are preset by the internodal distances between the Nodes of Ranvier and the maximum wave length will be determined by the strongest excitation at the internodal length. For $s_{\perp} = -1$ the wave excitation rate γ_e will be positive for $k > \kappa$ and will be increasing with the increase of the wave number k , hence shorter scale waves (often at the subthreshold level) and higher frequencies will be seen, i.e., more representative of unmyelinated Type II (and possibly some unmyelinated Type I as well) behavior.

F. Wave speeds and myelination

The dispersion relation allows the calculation of the wave phase velocity, the rate at which a wave of a single frequency propagates through the medium. The dimensional wave phase speed \mathcal{V} for the component along the axon from (14) is

$$\mathcal{V} \equiv \frac{\omega_k}{k} \Sigma^i d = \Lambda_{\parallel} \Sigma^i d \quad (24)$$

where the factor $\Sigma^i d$ appeared as the parameters have been converted to dimensional form. The simple estimates of wave phase velocity, in particular the dependence of the velocity on axon diameter d , show consistent behavior with both myelinated and unmyelinated conditions.

a. Myelinated axons For myelinated axons the ratio of the axon diameter to the total (axon and myelin) diameter is relatively constant (around 0.6–0.8) [23, 24] so that in our dimensionless units $\bar{\delta}_m \sim 0.2 – 0.4$. This determines the radial oscillation spatial wave number $\kappa_m \sim \pi/\bar{\delta}_m \sim 5 – 15$. As myelination makes the cross membrane conductivity (Σ_{rr}^0) smaller, it effectively decreases the wave damping γ_d for all scales smaller than the inter-node distance. Therefore, we may assume that the inter-node distance between the Nodes of Ranvier L_m determines the wavelength of the propagating modes. The inter-node distance between Nodes of Ranvier L_m can be as high as 1.5 mm, but typically ranges from 350 μm for

12 μm axon diameter, to 205 μm for 3.4 μm axon diameter [25], to 139 μm for 0.82 μm axon diameter [24] so that parallel spatial wave number $k_m \sim 2\pi/L_m \sim 0.005 – 0.05$ and $\kappa \gg k_m$ so that $\varkappa \approx \kappa$. Hence, for myelinated axons the wave phase speed is directly proportional to axonal diameter (assuming that $\Sigma'_{\parallel} = (x^2 + y^2)\hat{V}\Sigma'/2 \sim 0.05$, i.e., less than a maximum value of 1 due to multiple layers of myelin, d is in the units of μm , and a conversion factor from μm to m is included into the numerical constant)

$$\mathcal{V} = \Lambda_{\parallel} \Sigma^i d \sim 5 \times 10^3 \frac{\Sigma'_{\parallel}}{\bar{\delta}_m \kappa_m^2} d \sim (5 – 10)d \quad (25)$$

in units of m/s , giving values of 100–200 m/s for 20 μm diameter axons which is consistent with published values [26].

These results also provide an explanation for some recently detected anomalous phenomena of nerve conduction, such as the observations that in myelinated nerves the conduction velocity increases with stretch which contradicts existing theories since the diameter decreases on stretching [36]. However, this agrees well with our results as stretching increases the intra-nodal distance, hence increases both the wave length and the wave phase velocity (21).

b. Unmyelinated axons For unmyelinated axons the membrane diameter is constant $\delta_u \sim 10 \text{ nm} = 10^{-2} \mu\text{m}$ and the wavelength L_u of the propagating modes is going to be significantly smaller (depending on the small scale membrane geometry), but it is reasonable to assume $L_u \sim d/10$. That gives for the dimensionless wavenumber $k_u \sim 2\pi d/L_u \sim 20\pi \sim 10^2$, and κ_u is again determined by the same relation $\kappa_u \sim \pi/\bar{\delta}_u$, where $\bar{\delta}_u$ now is not fixed, $\bar{\delta}_u = \delta_u/d$. Then the expression to the wave speed as a function of d (assuming maximum value for $\Sigma'_{\parallel} \sim 1$, and both d and δ_u in the units of μm)

$$\mathcal{V} = \Lambda_{\parallel} \Sigma^i d \sim 5 \times 10^3 \frac{\Sigma'_{\parallel}}{\delta_u k_u^2} \frac{d^2}{1 + d^2 \pi^2 / (\delta_u^2 k_u^2)}, \quad (26)$$

giving roughly range from 0.5 to 5 m/s for axon diameters from 0.1 to 10 μm . Thus the wave speeds of myelinated axons are predicted to be around two orders of magnitude larger than unmyelinated axons. The importance of this analysis is not just that these predictions are consistent with measured values but that they were derived from first principles and therefore based on rather simple (at least to first order) measurable axon characteristics. This offers the potential for a better understanding of brain communication deficits associated with ubiquitous demyelinating diseases such as multiple sclerosis.

G. Diffusion limits of the cable theory

A standard accepted model for the propagation of the action potential spike is the so-called *cable theory*, an approach developed by Hodgkin and Rushton [27] to model

the passive conduction based on theoretical work on submarine telegraph cables by William Thompson (Lord Kelvin). This work was further developed and extended to dendritic spines by Rall [28, 29] who popularized this approach which has now become an established model in description of neuronal communication [30–33] with a host of variations, such as double cables [34, 35]. Because of the linear cable theory’s ubiquity and universal acceptance, we take a brief digression in this section to demonstrate that it is derivable from our more general theory described by (5) by making several simplifications. In doing so, we reveal that the standard cable theory does not actually support sustained propagation of the action potential in a wide range of experimentally reported physiological parameters.

a. Derivation of the cable equation from (5) The importance of tissue anisotropy and inhomogeneity and a full non-linear analysis to the generation of persistent surface waves is emphasized by the fact that the cable equation, which does *not* produce such waves, can be recovered from our general model (5) by ignoring important components that contribute to these properties, namely the non-diagonal and non-linear terms in the conductivity tensors.

Ignoring all non-diagonal and nonlinear terms in the conductivity tensors and assuming that only Σ_{\perp}^0 and Σ_{\parallel}^0 terms are non-zero, so that Σ in (4)

$$\Sigma \equiv \begin{pmatrix} \Sigma_{\perp}^0 & 0 \\ 0 & \Sigma_{\parallel}^0 \end{pmatrix}, \quad (27)$$

the equation for the electric field potential becomes, from (5),

$$\frac{\partial}{\partial t} \left(\frac{1}{r} \frac{\partial \phi}{\partial r} r + \frac{\partial^2 \phi}{\partial z^2} \right) = -\Sigma_{\perp}^0 \frac{1}{r} \frac{\partial \phi}{\partial r} - \Sigma_{\parallel}^0 \frac{\partial^2 \phi}{\partial z^2}. \quad (28)$$

As cable equation is not supposed to follow the exact radial dependence of the ϕ , we can use the above equation (28) and obtain its approximate form in the limit of a very thin lipid bilayer, i.e., $\bar{\delta} \ll 1$ and assuming that the largest radial variations of the potential ϕ are located around the membrane. This enables an approximate solution where the time dependence of the field is wholly contained in the axial dimension, while the radial component is constructed to meet some minimal boundary conditions based on simple geometric constraints. Therefore, we can search for the approximate solution separable in the radial and axial dimensions of the form $\phi = \phi'_r(r)\phi_a(z, t)$, where $\phi'_r(r) = -1 + \phi^0(r)$, i.e., -1 for $0 \leq r \leq 1$, transitions from -1 to 0 for $1 \leq r \leq 1 + \bar{\delta}$ and equals 0 for $r > 1 + \bar{\delta}$. Multiplying the equation (28) by $\phi'_r(r)r$ and integrating it from 0 to infinity we obtain the cable equation in the usual form [29, 31] as

$$\frac{1}{\bar{\delta}} \frac{\partial \phi_a}{\partial t} + \frac{\Sigma_{\perp}^0}{\bar{\delta}} \phi_a = \frac{\Sigma_{\parallel}^0}{2} \frac{\partial^2 \phi_a}{\partial z^2}, \quad (29)$$

where we used

$$\int_0^{\infty} \frac{1}{r} \frac{\partial \phi}{\partial r} r \frac{\partial \phi'_r}{\partial r} r dr = -\phi_a \int_1^{1+\bar{\delta}} \left| \frac{\partial \phi'_r}{\partial r} \right|^2 r dr \approx -\frac{\phi_a}{\bar{\delta}}, \quad (30)$$

$$\int_0^{\infty} \phi \phi'_r(r) r dr = \phi_a \int_0^{1+\bar{\delta}} |\phi'_r(r)|^2 r dr \approx \frac{\phi_a}{2}. \quad (31)$$

and have ignored the second term under time derivative in (28) because it is negligible when the axial scales of variation of the potential ϕ_a is larger than $\sqrt{\bar{\delta}/2}$. We thus recover the cable equation (29) from (28), where Σ_{\perp}^0 corresponds to the normalized membrane scaled conductivity and Σ_{\parallel}^0 equals to the normalized scaled conductivity of the axon internal fluid (i.e., $\Sigma_{\parallel}^0 \sim 1$ in dimensionless units). The terms in the equation (29) directly correspond to dissipative (no positive feedback) terms of Λ_{\perp} (15) to (17) in the limit $k^2 \ll \kappa^2 \sim 1/\bar{\delta}^2$.

b. Length and time scale of the cable equation The cable equation describes that the height of the action potential peak decays with time t as $\sqrt{t_0/t}$, where the shortest time $t_0 \sim 1/\Sigma_{\perp}^0$ corresponds to the narrowest

($\sqrt{\bar{\delta}/2}$) and the tallest ($\phi_a(t_0, z_0) = \phi_m$) shape of the action potential peak that the cable equation is capable of describing (and when the cable equation approximation is valid). The decay is actually even faster as it includes an exponential term $\exp(-\Sigma_{\perp}^0 t)$, but the approximate time dependence will be valid when $t < 1/\Sigma_{\perp}^0$ and, as the ratio of the cross membrane to the intracellular conductivities is very small (10^{-8} to 10^{-12}) [22], we can safely use this approximation in all our estimates below. The dimensionless diffusion coefficient is then equal to $\Sigma_{\parallel}^0 \bar{\delta}/2$, which allows us to find the time dependence for the axial diffusion length (the half width of the pulse) as $\Delta z \sim \sqrt{t \Sigma_{\parallel}^0 \bar{\delta}/2}$.

The ratio of the differences of the action potential firing threshold to the total peak above the resting potential in the HH-model is equal to about $\Delta \phi_a/\phi_m \sim 0.15$ (resting potential is -70 mV, threshold -55 mV, peak 30 mV). Therefore, the maximum time until the diffusively spreading pulse will be above threshold is about $\sim t_0 \phi_m^2 / \Delta \phi_a^2 \ll 1/\Sigma_{\perp}^0$, giving for the maximum diffusion length $\Delta z \sim \sqrt{\bar{\delta}/2 \phi_m / \Delta \phi_a}$.

c. Myelinated axons For a myelinated $20 \mu\text{m}$ diameter axon with the thickest myelin layer ($\bar{\delta} \sim 0.4$) this gives the maximum diffusion length of about $60 \mu\text{m}$, which is significantly shorter than the internodal length of $\sim 2\text{mm}$ between the Nodes of Ranvier of the typical $20 \mu\text{m}$ axon. Decreasing the myelin thickness will decrease the maximum propagation length even more. Naïve attempts to adjust the threshold parameters of HH-model to accommodate for longer maximum diffusion length will quickly reveal the significant model inconsistencies. For example, using the typical average ranges of internodal

distances for different axon diameters (350 μm for 12 μm axon diameter, 205 μm for 3.4 μm axon diameter [25], to 139 μm for 0.82 μm axon diameter [24]) it can be easily seen that it will require to decrease the firing threshold in 10 to 60 times ($350 \times 0.15/12/\sqrt{\bar{\delta}/2} \sim 10$, $205 \times 0.15/3.4/\sqrt{\bar{\delta}/2} \sim 20$, $139 \times 0.15/0.82/\sqrt{\bar{\delta}/2} \sim 60$), hence will require exceedingly (and unrealistically) low threshold voltages in the range of -68.5 to -69.75 mV instead of -55 mV for the resting potential of -70 mV. The conclusion is therefore that the amount of diffusion provided by standard cable theory to action potential spike generation by thresholded reactive HH mechanism with experimentally confirmed parameter values is generally incompatible with the process of saltatory conduction.

d. Unmyelinated axons For unmyelinated axon the original HH model assumes that there are 60 Na^+ channels and 18 K^+ channels for every μm^2 of membrane [37]. A more detailed analyses of variations of Na^+ channels density show that in unmyelinated hippocampal axons, the density increases tenfold from the soma with 2.6 channels/ μm^2 , through the proximal axon (25 channels/ μm^2), to the distal axon (46.1 channels/ μm^2) [38, 39]. Therefore, it can be safely assumed that the average linear distances between ion channels for unmyelinated axon change from about 0.1 μm to 0.7 μm ($\sim 1/\sqrt{2.6}$). For a 500 μm diameter giant squid axon with 10 nm membrane, like the one used by Hodgkin and Huxley in their seminal work, the maximum diffusion length is about $\sqrt{10^{-2}/2}/500 \times 500/0.15 \sim 10.5\mu\text{m}$, which is significantly above the average linear inter-channel distance of 0.1 μm , thus gives enough flexibility to successfully do a mind entertaining exercise of fitting diffusive and reactive processes together. But for thin unmyelinated pyramidal tract dendrites with around 0.2 μm diameter and 5 nm membrane thickness ($\bar{\delta} \sim 0.025$), the maximum propagation distance is about 0.15 μm , i.e., several times less than 5 Na^+ channels/ μm^2 and 5 K^+ channels/ μm^2 density of pyramidal neuron [40] would provide.

The conclusion is that the action potential propagation model described by cable theory is incompatible with experimentally measured physiological parameters of both myelinated and unmyelinated axons. On the contrary, our linear wave model developed from first principles using measured physiological tissue parameters is able to describe wave propagation in all these parameter ranges.

H. Non-linear wave analysis

The linear wave analysis above is sufficient to demonstrate the existence of sustained propagating waves along the axons. However, as demonstrated in our previous work [14, 15], a full non-linear analysis is necessary to accurately describe the details of the spatiotemporal characteristics of the propagating waves.

Proceeding as in [14, 15], the solution $\phi_w(z, t)$ is ex-

panded using a Fourier integral

$$\phi_w(z, t) = \int_{-\infty}^{\infty} a_k(t) e^{i(kz + \omega_k t)} dk + \text{c.c.}, \quad (32)$$

assuming that

$$\left| \frac{1}{a_k(t)} \frac{da_k(t)}{dt} \right| < \omega_k. \quad (33)$$

and where c.c. refers to the complex conjugate. This results in a set of coupled equations for time dependent complex amplitudes $a_k(t) \equiv a(k, t)$

$$\frac{da_k}{dt} = (\gamma_e - \gamma_d) a_k + \mathcal{N}_k, \quad (34)$$

that have the same general form as Equation 14 in [14], where

$$\mathcal{N}(\phi) = D_{\perp} \phi_w^2 + D \frac{d\phi_w^2}{dz} + D_{\parallel} \frac{d^2 \phi_w^2}{dz^2}, \quad (35)$$

$$\mathcal{N}_k = \frac{1}{2\pi} \int_{-\infty}^{\infty} \mathcal{N}(\phi) e^{-i(kz + \omega_k t)} dz, \quad (36)$$

where the normalization coefficients D_{\perp} , D_{\parallel} , and D are given in Appendix 2 by (58). The detailed evaluation of nonlinear input from multiple wave modes assuming a general quadratic form of nonlinearity was shown in detail for both non-resonant and resonant terms in [14, 15]. It was shown there for the first time that it is the inverse proportionality between frequencies and wave modes that allows calculation of the nonlinear input in a relatively simple analytical form, resulting in a simple nonlinear equation for wave amplitude $a_k(t)$. Following [18–20] this equation can be written in the general form

$$\frac{da_k}{dt} = \gamma_k a_k + \beta'_k a_k a_k^* + \beta_k a_k^2 - \alpha_k a_k (a_k a_k^*)^{1/2}, \quad (37)$$

where complex γ_k includes $\gamma_e - \gamma_d$ as a real part and ω_k as an imaginary part, and the parameters α , β , and β' can be evaluated following [14, 15] using coefficients in (34) and (35).

This solution to the non-linear problem can be directly applied to the case of the single axon, using experimentally measured physiological parameters, thus providing a more precise characterization of the propagating action potential. An example of a numerical solution of equation (37) for the non-resonant condition using $\beta'_k = \exp(i\pi/4)$, $\beta_k = 2 \exp(-i\pi/4)$, $\alpha_k = 3$, and $\gamma_k = 1.996 + i$ is shown in Fig. 2. The solution shows behavior in close agreement with a typical axonal action potential.

We emphasize that this result was derived from first principles based on the electrical properties of the axon without the need for an artificial reaction-diffusion model

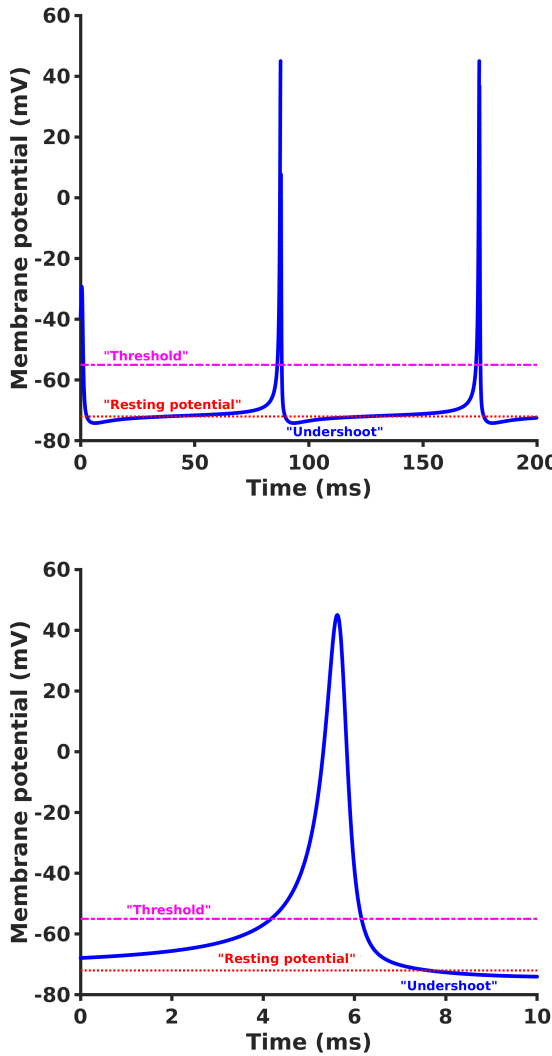


FIG. 2. An example of a numerical solution of equation (37) (top) and an expanded view of a single spike (bottom) using $\beta'_k = \exp(i\pi/4)$, $\beta_k = 2 \exp(-i\pi/4)$, $\alpha_k = 3$, and $\gamma_k = 1.996 + i$. The solution shows behavior in close agreement with typical axonal spiking but is derived directly from first principles of electrodynamics and wave propagation without any reference to the standard ad-hoc reaction-diffusion approach of HH.

with multiple adjustable parameters (thresholds, time constants, etc). In particular, equation (37) reveals that the inverse proportionality of frequency and wave number in the brain wave dispersion relation admits a closed analytical form of a wave nonlinear equation whose solution is a persistent traveling axonal nonlinear wave (i.e., the action potential spike) resulting from the collective non-resonant interactions of multiple low amplitude wave modes.

We note here that although we have assumed an idealized perfectly cylindrical model for clarity, the same formalism can be carried through with more complex geometries. However, it should also be recognized that the propagating nonlinear electrodynamic waves have the ca-

pability of deforming the geometry of the charged membrane, which is consistent with theoretical [41] and observational [42] evidence of mechanistic waves (APPulse [43, 44]) that accompany the action potential propagation.

I. Critical behavior of waves

1. Critical points

We have previously demonstrated in [18–20] that equation (37) can be rewritten in terms of a pair of coupled equations for the amplitude and phase as

$$\frac{dA}{dt} = \gamma A + A^2 [R_a \cos(\phi - \Phi) - \alpha], \quad (38)$$

$$\frac{d\phi}{dt} = \omega + AR_\phi \cos \phi, \quad (39)$$

where we omitted the subscript k from all variables and assumed $a(t) = A(t)e^{i\phi(t)}$. The parameters R_a , R_ϕ , and Φ can be expressed through β , and β' as shown in [18–20].

An equilibrium (i.e., $dA/dt = d\phi/dt = 0$) solution of (38) and (39) can be found from

$$-\frac{\gamma}{\omega} R_\phi \cos \phi + R_a \cos(\phi - \Phi) - \alpha = 0, \quad (40)$$

with equilibrium values $\phi_e \equiv \text{const}$ and $A_e = -\omega/R_\phi \cos \phi_e = -\gamma/(R_a \cos(\phi_e - \Phi) - \alpha) \equiv \text{const}$. This shows that for $\alpha > R_a |\sin \Phi|$ there exist critical values A_c , ϕ_c and μ_c ($\mu = \gamma/\omega$) where the equilibrium solution vanishes, such that

$$\begin{aligned} \mu_c &= \frac{R_a \cos(\phi_c - \Phi) - \alpha}{R_\phi \cos \phi_c} \\ &= \frac{1}{R_\phi} \left[R_a \cos \Phi \pm \sqrt{\alpha^2 - (R_a \sin \Phi)^2} \right] \end{aligned} \quad (41)$$

$$\begin{aligned} \phi_c &= \arctan \left[\frac{R_a \sin \Phi}{R_a \cos \Phi - \mu_c R_\phi} \right] \\ &= \arctan \left[\frac{R_a \sin \Phi}{\pm \sqrt{\alpha^2 - (R_a \sin \Phi)^2}} \right], \end{aligned} \quad (42)$$

$$A_c = -\frac{\omega}{R_\phi \cos \phi_c} = -\frac{\gamma}{\mu_c R_\phi \cos \phi_c}. \quad (43)$$

These solutions provide the basis for an analysis of the critical regimes via a bifurcation analysis.

2. Bifurcation analysis

The standard approach to analyzing the behavior of critical systems is to linearize the system equations around the critical point, then determine the stability of the system via the eigenvalues of the Jacobian (e.g.,

[45]). The linearized system of equations (38) and (39) at the critical point (A_c, ϕ_c) results in

$$\begin{aligned} \frac{dA}{dt} &= (\gamma + 2A_c [R_a \cos(\phi_c - \Phi) - \alpha]) A \\ &\quad - A_c^2 R_a \sin(\phi_c - \Phi) \phi, \end{aligned} \quad (44)$$

$$\frac{d\phi}{dt} = R_\phi \cos(\phi_c) A - A_c R_\phi \sin(\phi_c) \phi. \quad (45)$$

For different parameter ranges the system (44) and (45) (and hence the original system (38) and (39) or (37)) shows different behavior corresponding to different bifurcation types, including both the saddle node on an invariant circle (SNIC) bifurcation (representative for Type I axon spiking) and Hopf bifurcation (that is claimed to be responsible for Type II axon spiking) [46]. For example, taking a limiting case of $R_a \sim \alpha$ with $\Phi = 0$ (or $\Phi = \pi$) and $\phi_c = \pi$, the eigenvalues of the Jacobian matrix become

$$\lambda_1 = 0, \quad \lambda_2 = \gamma - 2\omega \frac{\alpha \pm R_a}{R_\phi}, \quad (46)$$

thus the system undergoes the SNIC bifurcation ($\lambda_1 = 0$ and $\lambda_2 < 0$ for $\mu < 2\mu_c$).

For an alternative limiting case of $R_a \ll \alpha$ with $\Phi = -\pi/2$ and $\phi_c \approx \pi$, the eigenvalues of the Jacobian matrix become

$$\lambda_{1,2} = q \pm \sqrt{q^2 - R_a/R_\phi} \quad (47)$$

$$q = \frac{\gamma}{2} - \omega \frac{\alpha}{R_\phi} \quad (48)$$

and in this case for $q = 0$ (or $\mu = 2\mu_c$) the eigenvalues $\lambda_{1,2}$ are pure imaginary, crossing the imaginary axis with a change of parameter μ (either ω or γ), which is an example of a Hopf bifurcation. Thus, the wave model of action potential shows that nonlinear axon wave includes multiple critical regimes and produces different spiking behavior consistent with different experimentally detected types.

It should be noted that the nonlinear system (38) and (39) is not a simple harmonic oscillator system. For a harmonic oscillator the amplitude A is constant (does not change at all) and the phase ϕ is changing rapidly with a constant rate ω . The nonlinear system (38) and (39) in the sub-critical regime, i.e., when $\mu < \mu_c$, shows the oscillations where the rate of phase change is not constant anymore and the amplitude A is changing as well, reaching the maximum $A_{max} = \gamma/(\alpha - R_a)$ and the minimum $A_{min} = \gamma/(\alpha + R_a)$ for $dA/dt = 0$ when $\phi = \Phi$ and $\phi = \Phi + \pi$ respectively.

3. Spike rate analysis

As in [18–20] we can estimate the effective period of spiking T_s (or its inverse – either the firing rate $1/T_s$ or

the effective firing frequency $2\pi/T_s$) from (39) by substituting A with either A_{min} (for positive spikes, $|\phi_c - \Phi| > \pi/2$) or A_{max} (for negative spikes, $|\phi_c - \Phi| < \pi/2$) as for the most of the time (except for the short spike duration time) the amplitude A will be close to one of those values, hence

$$\begin{aligned} T_s &= \int_0^{2\pi} \frac{d\phi}{\omega + \frac{\gamma R_\phi}{\alpha \pm R_a} \cos \phi} = \frac{1}{\omega} \int_0^{2\pi} \frac{d\phi}{1 + \frac{\mu}{\mu_c} \nu \cos \phi} \\ &= \frac{2\pi}{\omega \sqrt{1 - \nu^2 \mu^2 / \mu_c^2}}, \end{aligned} \quad (49)$$

where

$$\nu = \frac{R_a \cos(\phi_c - \Phi) - \alpha}{(\alpha \pm R_a) \cos \phi_c}, \quad (50)$$

and the effective firing frequency ω_s

$$\omega_s = \frac{2\pi}{T_s} = \omega \sqrt{1 - \nu^2 \mu^2 / \mu_c^2}. \quad (51)$$

As in the case discussed above where $\Phi = 0$ (or $\Phi = \pi$) and $\phi_c = \pi$ (also discussed in [18–20]) results in $\nu = 1$, hence gives $\omega_s = 0$ when μ reaches the critical value μ_c , that is it allows spiking with arbitrary low frequencies – the typical behavior of Type I neurons [46]. In the alternative case of $\Phi = -\pi/2$ and $\phi_c = \pi$, $\nu = \alpha/(\alpha + R_a) < 1$, hence at the critical point the spiking frequency ω_s can not be less than the minimum value of $\omega \sqrt{1 - \nu^2} > 0$ – the behavior attributed to Type II neurons [46].

4. Influence of the applied potential

Our construction of the conductivity tensor in (8) included an adjustable normalization V that represents the equilibrium voltage drop across the membrane because the vast majority of experiments investigating neuronal spiking involve some form of manipulation of V , such as “voltage clamping”. From dispersion relation expressions (14) to (17) and (21) it follows that

$$\mu = \frac{\gamma_e - \gamma_d}{\omega} = \mu_0 + \frac{\gamma_d}{\omega_0} \left(1 - \frac{V_0}{V} \right), \quad (52)$$

where μ_0 and ω_0 are the critical parameter and the linear wave frequency evaluated at $V = V_0$. Therefore in the sub-critical ($\mu < \mu_c$) regime increasing the voltage difference V across the membrane, or hyperpolarizing the membrane, increases the criticality parameter μ , hence decreases the firing frequency ω_s , stopping the oscillatory (spiking) behavior completely when the critical point μ_c is reached. In the super-critical ($\mu > \mu_c$) case, i.e., when the neuron is not firing, decreasing the voltage difference V (depolarizing the membrane as it is done in voltage clamping experiments) decreases the criticality parameter μ and makes neuron fire either at non-zero frequency

(similar to Type II neuron) or at arbitrary low frequency (similar to Type I neuron). A special case of a neuron firing a single spike at the critical point may also appear if an update of the cross membrane voltage proceeds too slowly and the system is able to relax back and stay at or above the critical point, but the periodic firing will emerge with increasing firing frequency ω_s when depolarization continues moving μ further in the sub-critical range.

5. Implications for neural networks

As shown in [13, 16, 17], the network organized from such nonlinear oscillators shows synchronization properties that neither linear oscillators nor diffusive-reactive HH neurons are capable of producing. Therefore, the current view that a single neuron can be approximated by the reactive HH system that is communicating through the cable-like diffusive signal propagation with other neurons in the networks of interconnected neurons may not be entirely appropriate for understanding the dynamics of brain communication. A more appropriate view may be to consider that the critical synchronized state is formed both at a single neuron level and in their interconnected networks by multiple waves that are constantly generated at axonal membranes, interact and propagate along those membrane interfaces, making the networks they form to be more appropriately analogous to webs of highly tensioned strings rather than networks of leaky pipes with slow diffusive flow of some substance inside those pipes.

In this “string theory” view of neural networks, all the specific details of the complex biochemical processes that mediate the membrane voltages are not seen as the actual mechanism behind axonal spiking nor the subsequent signal propagation in single neurons and networks of neurons. Rather, the details about opening and closing of voltage gated channels, about different number of Na^+ , K^+ , Cl^- , Ca^{2+} , etc., channels, about differences in kinetics of those carrier channels, about operation of ATP mediated carrier pumps, etc., all serve to “tune” the membranal strings by keeping the individual membranes, and hence, the network as a whole, at or close to the critical level.

III. CONCLUSION

Highly non-linear systems in nature present a significant problem in data analysis and interpretation because they can produce a wide variety of seemingly disparate and unrelated coherent phenomena. This is particularly true in critical systems where small parameter variations produced drastically different system configurations. Without a physical model for such systems, one is left with a confusing conglomeration of experimentally observed and often seemingly contradictory effects with-

out a guiding principle for understanding the underlying system dynamics. And without a guiding theoretical framework, data analysis strategies must often fall back on essentially *ad hoc* fitting methods. The more complex the system, the more parameters are required. Such strategies make it possible to fit the data, but deriving a link to the actual system dynamics in the absense of a theoretical framework is problematic.

The human brain is a spectacular example of such a non-linear critical system. But the lack of a physical theory of brain activity has led research down that familiar pathway. So while the pioneering work of Hodgkin and Huxley [1] provided a new unifying framework for fitting the action potential, it must be recognized for what it is: an *ad hoc* multiparameteric fitting method without a physical model. It is not surprising then that it has some glaring weaknesses, as noted above, not least of which is the difficulty in relating the neuronal action potential to large scale brain network communication. Nevertheless, it has remained the standard model for the action potential and forms the basis for subsequent methods that rely on the empirical fitting of a single measured axonal signal waveform to a set of *ad hoc* multi-parametric differential equations with multiple fitting parameters as is typically employed by a multitude of single-neuron spiking models [2–5, 10–12].

Our recent development of a general physical model (WETCOW) for brain activity derived from the first principles of electrodynamics [14–17] was motivated by the desire to address this problem by constructing a single unifying framework for understanding brain activity at all scales, from neuron to network. Subsequent papers focussed on the large scale effects such as network synchronization, learning, and neuronal avalanches [13, 19, 20]. While this model was developed with all neural tissues in mind, and therefore implicitly applicable to single neurons, we never explicitly solved this problem, which simply involved applying the general theory to the appropriate tissue model of a single neuron. The objective of this paper was to solve this problem and therefore explicitly demonstrate that our general theory works at the range of scales relevant to brain activity.

In doing so, we have demonstrated this theory of the neuron action potential is the same that has already demonstrated the ability to explain multiple observed macroscopic brain electric activity such as extracellular spiking, efficient brain synchronization, neuronal avalanches, and memory and learning mechanisms [13–16, 19, 20] that are not explained by the standard HH model. We have thus demonstrated a theory which bridges the gap between the most elemental brain electrical unit - the neuron, and the large scale collective synchronous behavior of the brain.

The construction of a physical theory from the first principles of electrodynamics begged the question of the relationship to existing electrodynamic models. The most obvious candidate is the ubiquitous ‘cable theory’ which has a long history in attempted descriptions of

neuronal signals. However, as we demonstrated in section II G, it is derivable from our more general theory but only by the imposition of conditions that limit its applicability to real neurons. The cable equations were subsequently shown to be inadequate to characterize the action potential under a wide range of realistic conditions.

Recognition that the HH model has never been capable of solving the problem of characterizing the action potential in myelinated axons led us to consider that problem within our theory. We found that the solution was straightforward because our theory explicitly incorporates both geometrical and physiological tissue parameters. This resulted in predictions for wave speeds consistent with measured values in both myelinated and unmyelinated axons. It should be noted that these results have practical significance because they provide a direct method for relating neuronal activity to disease states wherein demyelination exists, such as Multiple Sclerosis [47], and myelin pathogenesis, such as Alzheimer's Disease [48, 49].

The ability of our general WETCOW theory to describe both spatially extended (including network level) effects as well as neuron scale effects, led to the demonstration of some remarkable similarities between the two scales of brain phenomena. In section III we demonstrated that the critical behaviour previously shown to be evident in collective synchronous spiking and neuronal avalanches [18–20], was similarly manifest in the neuronal signal where now it corresponds to the characteristics of Type I and Type II neurons.

One obvious question these results raise is the logic of the current view of neuronal signaling being *created* by the HH mechanism of ion exchange, particularly in light of the demonstrated inadequacy of the diffusion picture. The traveling coherent non-linear waves predicted by our theory based solely on the bioelectric properties of the tissues will *cause* a time-dependent voltage drop across the neuronal membrane that will influence transmembrane permeability, and therefore have the ability to open and close multiple voltage gated channels in synchrony. In this view, the problematic question of how ion channels mysteriously synchronize to produce an action potential never arises.

ACKNOWLEDGEMENTS

LRF and VLG were supported by NSF grant ACI-1550405 and NIH grant R01 AG054049.

APPENDIX

1. Normalization constants

It is convenient to introduce normalization constants C_{\perp} , C_{\parallel} , and C for radial eigenmodes of the linear model as

$$C = \frac{1}{\kappa^2} \int_1^{1+\bar{\delta}} r \left[\frac{d\phi_r}{dr} \right]^2 dr = \int_1^{1+\bar{\delta}} r \phi_r^2 dr \\ = \bar{\delta} \int_0^1 (1 + \bar{\delta}r) \phi_r^2 dr \approx \bar{\delta} \int_0^1 \phi_r^2 dr, \quad (53)$$

$$C_{\perp}^r = \frac{1}{\kappa^2} \int_1^{1+\bar{\delta}} r \ln r \left[\frac{d\phi_r}{dr} \right]^2 dr, \quad (54)$$

$$C_{\perp}^z = \int_1^{1+\bar{\delta}} r \ln r \phi_r^2 dr, \quad (55)$$

$$C_{\perp}^r \approx C_{\perp}^z = \bar{\delta} \int_0^1 (1 + \bar{\delta}r) \ln(1 + \bar{\delta}r) \phi_r^2 dr \approx \frac{\bar{\delta}}{2} C, \quad (56)$$

$$C_{\parallel} = \int_1^{1+\bar{\delta}} \frac{d(r \ln r)}{dr} \phi_r^2 dr \\ = \bar{\delta} \int_0^1 (1 + \ln(1 + \bar{\delta}r)) \phi_r^2 dr \approx C. \quad (57)$$

2. Normalized coefficients

It is also convenient to introduce normalization coefficient D_{\perp} , D_{\parallel} , and D for the nonlinear model as

$$D_{\parallel} = -\frac{\Sigma'_{zz}}{2C\kappa^2} \int_1^{1+\bar{\delta}} r \phi_r^3 dr, \\ D_{\perp} = \frac{\Sigma'_{rr}}{C\kappa^2} \int_1^{1+\bar{\delta}} r \phi_r \left[\frac{d\phi_r}{dr} \right]^2 dr, \\ D = \frac{(2\Sigma'_{zr} - \Sigma'_{rz})}{6C\kappa^2} \int_1^{1+\bar{\delta}} \phi_r^3 dr, \quad (58)$$

where κ^2 is given by (19). and the normalization parameters C_{\perp} , C_{\parallel} , and C are provided in Appendix 1 by (53).

[1] A. L. Hodgkin and A. F. Huxley, A quantitative description of membrane current and its application to conduction and excitation in nerve, *J. Physiol. (Lond.)* **117**, 500 (1952).

[2] R. Fitzhugh, Impulses and Physiological States in Theoretical Models of Nerve Membrane, *Biophys. J.* **1**, 445 (1961).

[3] J. Nagumo, S. Arimoto, and S. Yoshizawa, An active pulse transmission line simulating nerve axon, *Proceedings of the IRE* **50**, 2061 (1962).

[4] C. Morris and H. Lecar, Voltage oscillations in the barnacle giant muscle fiber, *Biophys. J.* **35**, 193 (1981).

[5] E. M. Izhikevich, Simple model of spiking neurons, *IEEE Trans Neural Netw* **14**, 1569 (2003).

[6] G. Buzsaki, *Rhythms of the Brain* (Oxford University Press, 2006).

[7] A. F. Strassberg and L. J. DeFelice, Limitations of the Hodgkin-Huxley formalism: Effects of single channel kinetics on transmembrane voltage dynamics, *Neural Comput.* **5**, 843 (1993).

[8] C. Meunier and I. Segev, Playing the devil's advocate: is the Hodgkin-Huxley model useful?, *Trends Neurosci.* **25**, 558 (2002).

[9] K. Yamazaki, V.-K. Vo-Ho, D. Bulsara, and N. Le, Spiking neural networks and their applications: A review, *Brain Sci.* **12**, 863 (2022).

[10] W. Gerstner, W. M. Kistler, R. Naud, and L. Paninski, *Neuronal Dynamics: From Single Neurons to Networks and Models of Cognition* (Cambridge University Press, New York, NY, USA, 2014).

[11] A. Kulkarni, J. Ranft, and V. Hakim, Synchronization, Stochasticity, and Phase Waves in Neuronal Networks With Spatially-Structured Connectivity, *Front Comput Neurosci* **14**, 569644 (2020).

[12] R. Kim and T. J. Sejnowski, Strong inhibitory signaling underlies stable temporal dynamics and working memory in spiking neural networks, *Nat Neurosci* **24**, 129 (2021).

[13] V. L. Galinsky and L. R. Frank, Critically synchronized brain waves form an effective, robust and flexible basis for human memory and learning, *Sci Rep* **13**, 4343 (2023).

[14] V. L. Galinsky and L. R. Frank, Universal theory of brain waves: from linear loops to nonlinear synchronized spiking and collective brain rhythms, *Physical Review Research* **2**, 023061 (2020).

[15] V. L. Galinsky and L. R. Frank, Brain Waves: Emergence of Localized, Persistent, Weakly Evanescence Cortical Loops, *J. of Cognitive Neurosci* **32**, 2178 (2020).

[16] V. L. Galinsky and L. R. Frank, Collective synchronous spiking in a brain network of coupled nonlinear oscillators, *Phys. Rev. Lett.* **126**, 158102 (2021).

[17] V. L. Galinsky and L. R. Frank, Collective synchronous spiking in a brain network of coupled nonlinear oscillators, eprint arXiv:2104.02171 (2021).

[18] V. L. Galinsky and L. R. Frank, Neuronal avalanches and critical dynamics of brain waves, eprint arXiv:2111.07479 (2021).

[19] V. L. Galinsky and L. R. Frank, Critical brain wave dynamics of neuronal avalanches, *Frontiers in Physics* **11** (2023).

[20] V. L. Galinsky and L. R. Frank, Neuronal avalanches: sandpiles of self organized criticality or critical dynamics of brain waves?, *Frontiers of Physics* **18**, 45301 (2023).

[21] A. C. Scott, The electrophysics of a nerve fiber, *Rev. Mod. Phys.* **47**, 487 (1975).

[22] C. Bédard, H. Kröger, and A. Destexhe, Modeling extracellular field potentials and the frequency-filtering properties of extracellular space, *Biophys. J.* **86**, 1829 (2004).

[23] M. J. Gillespie and R. B. Stein, The relationship between axon diameter, myelin thickness and conduction velocity during atrophy of mammalian peripheral nerves, *Brain Res.* **259**, 41 (1983).

[24] I. L. Arancibia-Cárcamo, M. C. Ford, L. Cossell, K. Ishida, K. Tohyama, and D. Attwell, Node of ranvier length as a potential regulator of myelinated axon conduction speed, *Elife* **6** (2017).

[25] S. G. Waxman and R. J. Melker, Closely spaced nodes of ranvier in the mammalian brain, *Brain Res.* **32**, 445 (1971).

[26] A. Siegel and H. N. Sapru, *Essential Neuroscience* (Lippincott Williams and Wilkins, Philadelphia, PA, 2005) p. 257.

[27] A. L. Hodgkin, W. A. H. Rushton, and E. D. Adrian, The electrical constants of a crustacean nerve fibre, *Proceedings of the Royal Society of London. Series B - Biological Sciences* **133**, 444 (1946).

[28] W. Rall, Theory of physiological properties of dendrites, *Annals of the New York Academy of Sciences* **96**, 1071 (1962).

[29] W. Rall, Core conductor theory and cable properties of neurons, in *Comprehensive Physiology* (John Wiley & Sons, Inc., Hoboken, NJ, USA, 2011).

[30] I. Segev and M. London, Untangling dendrites with quantitative models, *Science* **290**, 744 (2000).

[31] W. R. Holmes, Cable equation, in *Encyclopedia of Computational Neuroscience* (Springer New York, New York, NY, 2014) pp. 1–13.

[32] M. Pagkalos, S. Chavlis, and P. Poirazi, Introducing the dendrify framework for incorporating dendrites to spiking neural networks, *Nature Communications* **14**, 131 (2023).

[33] N. Spruston, M. Häusser, and G. Stuart, Chapter 11 - information processing in dendrites and spines, in *Fundamental Neuroscience (Fourth Edition)*, edited by L. R. Squire, D. Berg, F. E. Bloom, S. du Lac, A. Ghosh, and N. C. Spitzer (Academic Press, San Diego, 2013) fourth edition ed., pp. 231–260.

[34] C. C. H. Cohen, M. A. Popovic, J. Klooster, M.-T. Weil, W. Möbius, K.-A. Nave, and M. H. P. Kole, Saltatory conduction along myelinated axons involves a periaxonal nanocircuit, *Cell* **180**, 311 (2020).

[35] B. C. Lim and M. N. Rasband, Saltatory conduction: Jumping to new conclusions, *Curr. Biol.* **30**, R326 (2020).

[36] S. Sharmin, M. A. S. Karal, Z. B. Mahbub, and K. S.-E. Rabbani, Increase in conduction velocity in myelinated nerves due to stretch - an experimental verification, *Front. Neurosci.* **17**, 1084004 (2023).

[37] B. Sengupta, A. A. Faisal, S. B. Laughlin, and J. E. Niven, The effect of cell size and channel density on neuronal information encoding and energy efficiency, *J. Cereb. Blood Flow Metab.* **33**, 1465 (2013).

[38] H. Hu and P. Jonas, A supercritical density of na(+) channels ensures fast signaling in GABAergic interneuron axons, *Nat. Neurosci.* **17**, 686 (2014).

- [39] S. A. Freeman, A. Desmazières, D. Fricker, C. Lubetzki, and N. Sol-Foulon, Mechanisms of sodium channel clustering and its influence on axonal impulse conduction, *Cell. Mol. Life Sci.* **73**, 723 (2016).
- [40] P. Arhem, G. Klement, and C. Blomberg, Channel density regulation of firing patterns in a cortical neuron model, *Biophys. J.* **90**, 4392 (2006).
- [41] A. El Hady and B. B. Machta, Mechanical surface waves accompany action potential propagation, *Nat. Commun.* **6**, 6697 (2015).
- [42] T. Ling, K. C. Boyle, G. Goetz, P. Zhou, Y. Quan, F. S. Alfonso, T. W. Huang, and D. Palanker, Full-field interferometric imaging of propagating action potentials, *Light Sci. Appl.* **7**, 107 (2018).
- [43] A. S. Johnson and W. Winlow, The soliton and the action potential – primary elements underlying sentience, *Front. Physiol.* **9** (2018).
- [44] A. Johnson and W. Winlow, Mysteries of the action potential, *Physiology News* , 38 (2018).
- [45] S. H. Strogatz, *Nonlinear Dynamics and Chaos: With Applications to Physics, Biology, Chemistry and Engineering* (Westview Press, 2000).
- [46] S. A. Prescott, Excitability: Types i, II, and III, in *Encyclopedia of Computational Neuroscience* (Springer New York, New York, NY, 2014) pp. 1–7.
- [47] V. G. Coutinho Costa, S. E.-S. Araújo, S. V. Alves-Leon, and F. C. A. Gomes, Central nervous system demyelinating diseases: glial cells at the hub of pathology, *Frontiers in Immunology* **14** (2023).
- [48] Z. Cai and M. Xiao, Oligodendrocytes and alzheimer’s disease, *International Journal of Neuroscience* **126**, 97 (2016).
- [49] M. Maitre, H. Jeltsch-David, N. G. Okechukwu, C. Klein, C. Patte-Mensah, and A.-G. Mensah-Nyagan, Myelin in alzheimer’s disease: culprit or bystander?, *Acta Neuropathologica Communications* **11**, 56 (2023).
- [50] J. Fraser, R. Horgan, D. Miller, A. Johnson, and B. Winlow, On the topic of mysteries of the action potential, *Physiology News* , 6 (2019).